Mechanical Systems and Signal Processing 26 (2012) 128–140

Contents lists available at ScienceDirect

Mechanical Systems and Signal Processing

journal homepage: www.elsevier.com/locate/ymssp

Characterize highly oscillating frequency modulation using generalized Warblet transform

Y. Yang, Z.K. Peng*, G. Meng, W.M. Zhang

State Key Laboratory of Mechanical System and Vibration, Shanghai Jiao Tong University, Shanghai 200240, PR China

ARTICLE INFO

Article history:
Received 26 September 2010
Received in revised form
27 April 2011
Accepted 23 June 2011
Available online 3 August 2011

Keywords:
Chirplet transform
Warblet transform
Generalized Warblet transform time-frequency analysis
Instantaneous frequency

ABSTRACT

In this paper, in order to characterize highly oscillating time-frequency patterns of signals, whose instantaneous frequency (IF) is periodic or non-periodic, a generalized Warblet transform (GWT) is proposed. By replacing sine function kernel of conventional Warblet transform with Fourier series function, the GWT is able to generate a time-frequency representation (TFR) with satisfying energy concentration for such signals. As any oscillating function can be well approximated by a Fourier series, the GWT is guaranteed to provide an effective way to achieve accurate IF estimation. In addition, a signal-dependent iterative procedure for coefficients estimation is developed to enable the GWT to be applied in practice. Using the Fourier spectrum of the IF, the coefficients of the Fourier series kernel function of the GWT can be estimated and refined adaptively. The effectiveness of the proposed method is verified through comparing with other time-frequency analysis methods on several numerical examples and experimental vibration signal, which is collected from a rotor test rig undergoing speed-up and slow-down stages.

1. Introduction

It is well known that frequency modulation (FM) signal conveys information over a carrier wave by varying instantaneous frequency (IF). The IF is a basic parameter of the time-frequency pattern of mono-component signals [1–3]. According to the time-frequency nature, FM signals can be categorized into the two classes: linear FM (LFM) signals and nonlinear FM (NLFM) signals. The LFM signal has linearly time-varying IF and the IF of NLFM signal is a nonlinear function of time. LFM signals are encountered in wide research areas, i.e., oceanic investigation [4], biomedical application [5], power system [6], and radar [7], sonar [8], telecommunication [9,10] and so on. NLFM signals are also frequently encountered in radar system [11,12], sonar [13], oceanic investigation [14], and machine health monitoring [15].

Time-frequency representation (TFR) obtained by time-frequency transform is a powerful tool to effectively characterize the time-frequency pattern of FM signals [16]. Most researches have focused on the analysis of signals with linearly time-varying IF. Commonly used time-frequency analysis (TFA) methods [17] include short-time Fourier transform (STFT), Wavelet transform (WT), and Wigner–Ville distribution (WVD). Since prior knowledge about the signal to be analyzed is not required, these TFA methods can be regarded as non-parameterized time-frequency transform. Specifically, the STFT [18,19] is a window-depending Fourier transform. By assuming the signal in the analysis window to be stationary, the local frequency is linearly approximated by a horizontal line. Thus, the STFT is only suitable to analyze the stationary and quasi-stationary signal with fixed time-frequency resolution. The WT [20–22] improves the STFT by providing scalable time-frequency resolution, i.e., finer frequency resolution at lower frequency, and finer time resolution at higher frequency. Despite that, the WT would result in worse time resolution at lower frequency and worse frequency resolution at higher frequency in the analysis of the signal with highly oscillating IF.

* Corresponding author. Tel.: +86 21 34206332 810.
E-mail address: pengzhike@tsinghua.org.cn (Z.K. Peng).

0888-3270/$ - see front matter Crown Copyright © 2011 Published by Elsevier Ltd. All rights reserved.
doi:10.1016/j.ymssp.2011.06.020

The WVD [23–25] can generate TFR with great energy concentration for LFM signals. Nonetheless, the cross-terms introduced by the bilinear structure of the WVD would mislead the time-frequency interpretation for the NLFM signal with highly oscillating IF.

Comparing to the non-parameterized TFA methods, parameterized time-frequency transforms, such as the Chirplet transform (CT) [26–28] and Warblet transform (WBT) [29], require the prior knowledge about signals to determine the parameter values of transform kernel function. When the kernel function well presents the IF trajectory of the signal, the parameterized time-frequency transforms will be much more effective in characterizing the time-frequency patterns of FM signals by providing a TFA with satisfying energy concentration, including the NLFM signals. By introducing an extra chirp kernel characterized by a chirping rate parameter, the CT is particularly developed to analyze LFM signals. To analyze signals, whose IFs are not exactly linear function of time, Angrisani and D'Arco [30] introduced a curvature parameter into the traditional CT, which provides a new degree of freedom for shaping the time-frequency cell. The modified version of the CT is able to analyze the signal, whose IF can be approximated by a nonlinear function characterized by the chirping rate and the curvature parameter. Even so, for the signal with highly oscillating IF that cannot be simply described by the chirping rate and the curvature parameter, the method cannot guarantee an enhancement for the estimation accuracy of the IF. The WBT adopts a sine kernel function so that it can deal with NLFM signals with sinusoidal-like IF law and provide well-concentrated TFR for such signals. Angrisani et al. [31] applied the WBT to analyze non-stationary signals for telecommunication systems. However, although the WBT can present excellent result for the signals with periodically changing IF law, it is not suitable to analyze the NLFM signals whose IF laws are not periodic.

In this paper, by introducing a frequency rotation operator and a frequency shift operator using Fourier series as kernel function, a generalized Warblet transform (GWT) is proposed. It is designed to characterize the time-frequency patterns for signals with arbitrary highly oscillating IF that can be approximated by Fourier series. Moreover, a signal-dependent iterative procedure is developed based on the spectrum of the objective IF, which can adaptively estimate and refine the coefficients of the Fourier series kernel functions for the GWT. This procedure enables the GWT to be applied in practice.

In Section 2, a frequency rotation operator and a frequency shift operator are first addressed, which have actually been used in the conventional CT but none has clearly revealed their existence before, and then the two operators are extended to the conventional WBT, which yields the GWT. The iterative signal-dependent coefficient estimation procedure for the GWT is presented in Section 3. In Section 4, the performance of the GWT is verified by comparing with other time-frequency transform methods on numerical examples and vibration signal collected from a test rig undergoing speed-up and slow-down stages. The conclusions are drawn in Section 4.

2. Generalized Warblet transform

This section starts with the CT, from which a frequency rotation operator and a frequency shift operator are proposed, and then these operators are extended to conventional WBT. The principles of the proposed GWT are then introduced.

2.1. Chirplet transform

The CT [26] is an effective method to analyze LFM signals, which is defined as follows:

$$CT(t_0,\omega,\alpha;\sigma)=\int_{-\infty}^{\infty} z(t)\Psi(t,t_0,\alpha,\sigma)\exp(-j\omega t)dt \tag{1}$$

where $z(t)$ is analytical signal of signal $s(t)$, $s(t)\in L^2(R)$, which is generated by a Hilbert transform [32], $\boldsymbol{H}$, i.e., $z(t)=s(t)+j\boldsymbol{H}[s(t)]$. $\Psi(t,t_0,\alpha,\sigma)$ is a complex window given as

$$\Psi(t,t_0,\alpha,\sigma)=w_{(\sigma)}(t-t_0)\exp\left[-j\frac{\alpha}{2}(t-t_0)^2\right] \tag{2}$$

where $t_0,\alpha\in R$ stand for time and chirping rate, respectively; $w\in L^2(R)$ denotes a window function, which is usually taken as a Gaussian function expressed as

$$w_\sigma(t)=\frac{1}{\sqrt{2\pi}}\sigma\exp\left[-\frac{1}{2}\left(\frac{t}{\sigma}\right)^2\right] \tag{3}$$

where σ determines the length of the Gaussian window.

According to the definition in Eqs. (1) and (2), the CT can be rewritten as

$$CT(t_0,\omega,\alpha;\sigma)=A(t_0)\int_{-\infty}^{\infty}\bar{z}(t)w_\sigma(t-t_0)\exp(-j\omega t)dt \tag{4}$$

with

$$\begin{cases}\bar{z}(t)=z(t)\Phi_\alpha^R(t)\Phi_\alpha^S(t,t_0)\\ \Phi^R(t,\alpha)=\exp(-j\alpha t^2/2)\\ \Phi^S(t,t_0,\beta)=\exp(j\alpha t_0 t)\\ A(t_0,\alpha)=\exp(-jt_0^2\alpha/2)\end{cases} \tag{5}$$

in which $\Phi^R(t,\alpha)$ is frequency rotation operator and $\Phi^S(t,t_0,\alpha)$ is frequency shift operator. $A(t_0)$ is a complex number with modulus $|A(t_0)|=1$. In the time-frequency analysis, the modulus of the TFR, i.e., $|CT(t_0,\omega,\alpha;\sigma)|$, which is usually of interests and meaningful. As indicated in Eqs. (4) and (5), the CT can be decomposed into three operators: (1) frequency rotation operator; (2) frequency shift operator; (3) STFT operator with the window $w_\sigma(t)$. Fig. 1 illustrates the procedure of the CT, in which the IF law of the objective signal is denoted as IF(t). First, the frequency rotation operator rotates the analytical signal $z(t)$ by an angle of arctan $(-\alpha)$ in the time-frequency plane. Then the frequency shift operator relocates the frequency component at t_0 by a frequency increment of αt_0. It is worth noting here that the frequency resolution of the CT depends on the chirping rate α and the length of the Gaussian window σ. For a signal with IF law of $\omega_0+\lambda_0 t$, the frequency resolution of the TFR generated by the CT is $\sigma|\lambda_0-\alpha|+(1/\sigma)$ and $|CT(t_0,\omega,\alpha;\sigma)|$ reaches the global maximum at $(\omega,\alpha)=(\omega_0,\lambda_0)$.

To illustrate the capability of the CT in dealing with the LFM signal, a signal consisting of two chirping frequency components is considered

$$s(t)=\sin[2\pi(5+2.5t)t]+\sin[2\pi(10+2.5t)t] \tag{6}$$

whose IF is $5+5t$ (Hz) and $10+5t$ (Hz). The sampling frequency is 200 Hz, the window length is 512 and the chirping rate is $\alpha=5$ (Hz/s). The TFRs generated by the STFT and CT are shown in Fig. 2.

In the TFR generated by the STFT shown in Fig. 2(a), the two IF trajectories cannot be distinguished for the poor time and frequency resolutions. Clearly, it is much easier for the TFR generated by the CT as shown in Fig. 2(b) to separate the two chirping frequency components. However, the CT is not suitable to analyze NLFM signals because of the linear kernel.

2.2. Warblet transform

The WBT is specifically designed to analyze the FM signal with periodic IF law. By applying the frequency rotation operator and the frequency shift operator with a sine kernel function, the WBT is presented as follows:

$$WT(t_0,w,\beta_m,f_m;\sigma)=\int_{-\infty}^{\infty}\bar{z}(t)w_\sigma(t-t_0)\exp(-j\omega t)dt \tag{7}$$

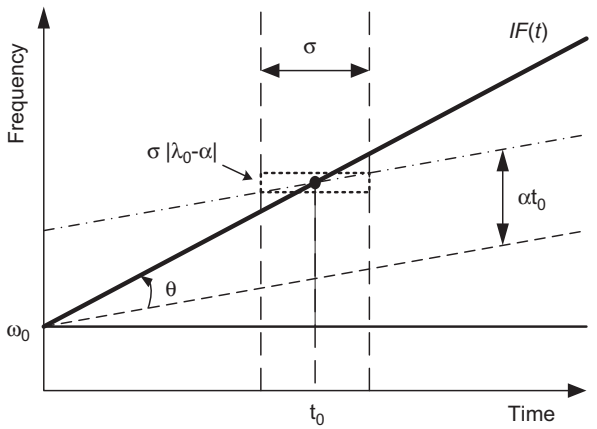

Fig. 1. The illustration of CT (solid line: the IF law of the object chirp signal; dash line: after frequency rotation; dash dot line: after frequency shift).

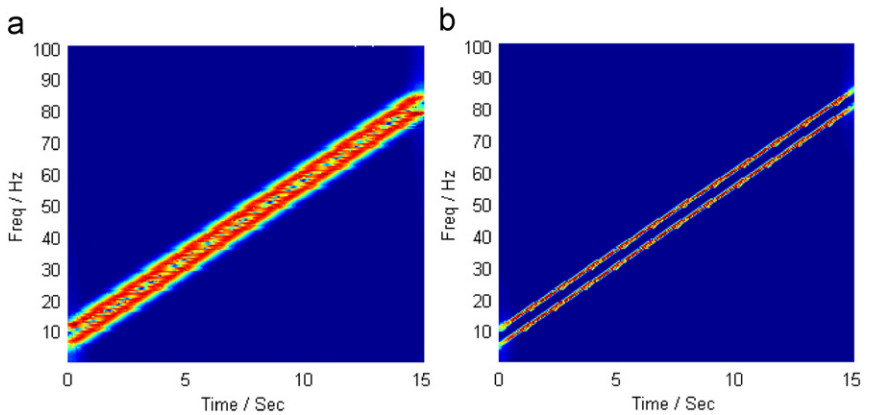

Fig. 2. The TFRs generated by (a) STFT and (b) CT ($\alpha=2.5$) for the signal given by Eq. (6).

with

$$\begin{cases} \bar{z}(t) = z(t)\Phi^R(t)\Phi^S(t,t_0) \\ \Phi^R(t,\beta_m,f_m) = \exp\left[-j\frac{\beta_m}{f_m}\sin(2\pi f_m t)\right] \\ \Phi^S(t,t_0,\beta_m,f_m) = \exp[j2\pi\beta_m\cos(2\pi f_m t_0)t] \end{cases} \tag{8}$$

in which f, β_m and f_m are carrier frequency, modulation amplitude and modulation frequency, respectively. In essence, the WBT applies the STFT to the objective signal after rotating and shifting operation. The signal is (1) rotated by subtracting the IF of $\Phi^R(t,\beta_m,f_m)$, i.e., $\rho=\beta_m\cos(2\pi f_m t)$ (Hz), from the IF of the objective signal in the time-frequency plane, and (2) relocated by adding the frequency of $\Phi^S(t,t_0,\beta_m,f_m)$ at time t_0, i.e., $\gamma=\beta_m\cos(2\pi f_m t_0)$ (Hz) in the time-frequency plane, and (3) processed by the STFT. The key steps of the WBT are illustrated in Fig. 3, where $\Delta\mathrm{IF}(t;\sigma)$ denotes the frequency range of IF $(t)-\rho$ in the Gaussian window. The frequency resolution is determined by $\Delta\mathrm{IF}(t;\sigma)$ and the bandwidth of Gaussian window $1/\sigma$. When the sine kernel well matches the IF of interest, $\Delta\mathrm{IF}(t;\sigma)$ will equal zero all over the time, and the frequency resolution of the WBT will be minimized to be $1/\sigma$.

To demonstrate the performance of the WBT in the analysis of the signal with periodic IF law, below FM signal is considered

$$s(t)=\sin(20\pi t+48\sin(t)) \tag{9}$$

whose IF law is $10+(24\cos(t)/\pi)$ (Hz). The CT and the STFT are considered for comparison purpose. The sampling frequency is 100 Hz, the chirp rate is $\alpha=16/\pi$ and the length of the window is 512. The parameters of the WBT are $\beta_m=24/\pi$ and $f_m=1/2\pi$. The TFRs generated by STFT, CT and WBT are shown in Fig. 4.

Clearly, neither STFT nor CT is able to achieve accurate estimation for the objective IF due to the fixed time-frequency resolution or the linear kernel function. On the contrary, the WBT shows remarkable capability of capturing the time-frequency characteristics of the signal as illustrated in Fig. 4(c), because the IF is well approximated by the sine kernel function. However, the WBT is not qualified to analyze signals with highly oscillating IF that cannot be approximated by single sine function.

2.3. Generalized Warblet transform

In order to analyze the signal with arbitrary highly oscillating IF which is periodic or non-periodic, the generalized Warblet transform is proposed to characterize the time-frequency patterns of such signals. As any oscillating function can be well approximated by a Fourier series, the GWT assures the accurate IF estimation for the signal by replacing the sine kernel of the frequency rotation operator and the frequency shift operator of the WBT with Fourier series as follows:

$$GWT(t_0,a,\beta,f,\omega;\sigma)=\int_{-\infty}^{\infty}\bar{z}(t)w_\sigma(t-t_0)\exp(-j\omega t)dt \tag{10}$$

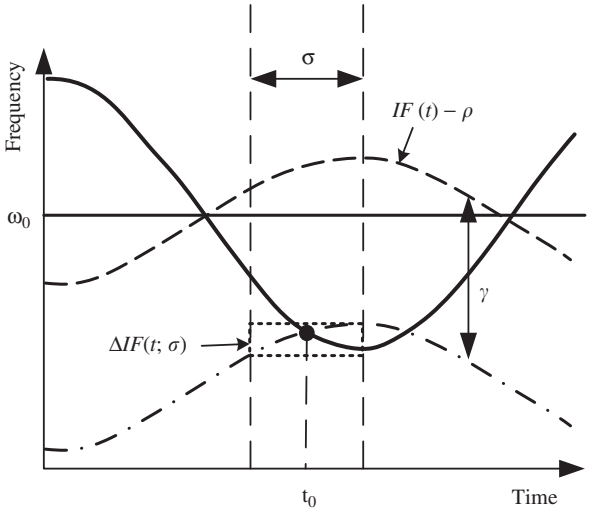

Fig. 3. The illustration of WBT (solid line: the IF law of the object chirp signal; dash line: after frequency rotation; dash dot line: after frequency shift).

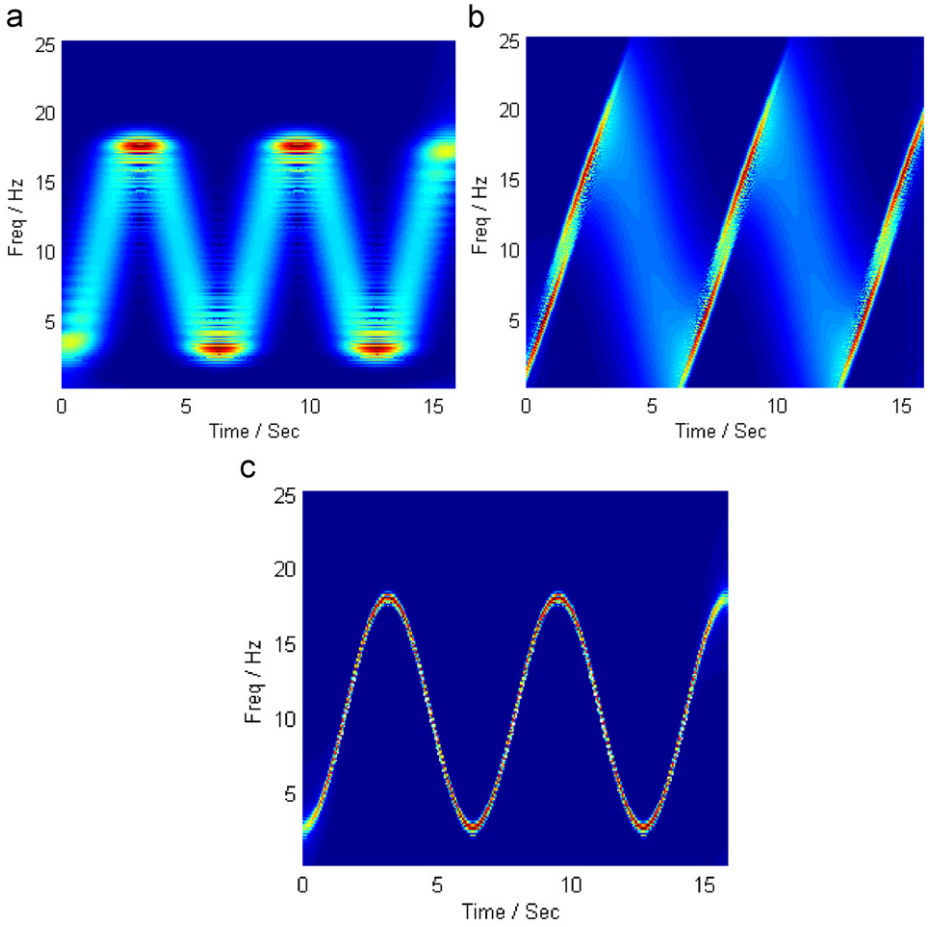

Fig. 4. The TFRs generated by (a) STFT, (b) CT ($\alpha=16/\pi$) and (c) WBT ($\beta_m=-24/\pi, f_m=1/2\pi$) for the signal given by Eq. (9).

with

$$\begin{cases} \bar{z}(t)=z(t)\Phi^R(t,a,\beta,f)\Phi^S(t,t_0,a,\beta,f) \\ \Phi^R(t,a,\beta,f)=\exp\left[-j\left(\sum_{i=1}^{m}\frac{a_i}{fi}\cos 2\pi f_i t+\sum_{i=1}^{m}\frac{\beta_i}{f_i}\sin 2\pi f_i t\right)\right] \\ \Phi^S(t,t_0,a,\beta,f)=\exp\left[j2\pi\left(-\sum_{i=1}^{m}a_i\sin 2\pi f_i t_0+\sum_{i=1}^{m}\beta_i\cos 2\pi f_i t_0\right)t\right] \end{cases} \tag{11}$$

in which m is total number of the sine or cosine functions $\{a_1,a_2,...,a_m\}$ and $\{\beta_1,\beta_2,...,\beta_m\}$ are Fourier coefficients. $\{f_1,f_2,...,f_m\}$ is the corresponding frequencies. $\Phi^R(t,a,\beta,f)$ and $\Phi^S(t,t_0,a,\beta,f)$ are the frequency rotation and frequency shift operators, respectively. First, the frequency rotation operator rotates the analytical signal by subtracting the IF of $\Phi^R(t,a,\beta,f)$, i.e., $\rho=(-\sum_{i=1}^{m}a_i\sin 2\pi f_i t+\sum_{i=1}^{m}\beta_i\cos 2\pi f_i t)$ (Hz) from the IF of the signal, and then, the frequency shift operator shifts the frequency component at time t_0 by adding the frequency of $\Phi^S(t,t_0,a,\beta,f)$, i.e., $\gamma=(-\sum_{i=1}^{m}a_i\sin 2\pi f_i t_0+\sum_{i=1}^{m}\beta_i\cos 2\pi f_i t_0)$ (Hz), and then, the STFT with window w_σ is applied.

The procedure of the GWT is illustrated in Fig. 5. When the Fourier series well matches the objective IF, the frequency range of IF$(t)-\rho$, i.e., $\Delta\mathrm{IF}(t;\sigma)$, will be zero in the Gaussian window, and the frequency resolution will reach the minimum, i.e., $1/\sigma$. It is noticed that when $\{a_1,a_2,...,a_m\}=\{0,0,...,0\}_{1\times m}$ and $\{\beta_1,\beta_2,...,\beta_m\}=\{0,0,...,0\}_{1\times m}$, the GWT degenerates to the STFT. When $m=1$, the GWT degenerates to the conventional WBT, thus the Warblet transform is the special case of the GWT.

3. Coefficient estimation method for GWT

It was addressed that the properly determined coefficients can make the Fourier series kernel of the GWT well match the IF of the signal. With the proper Fourier series kernel, the GWT is able to characterize the time-frequency pattern of signals, whose

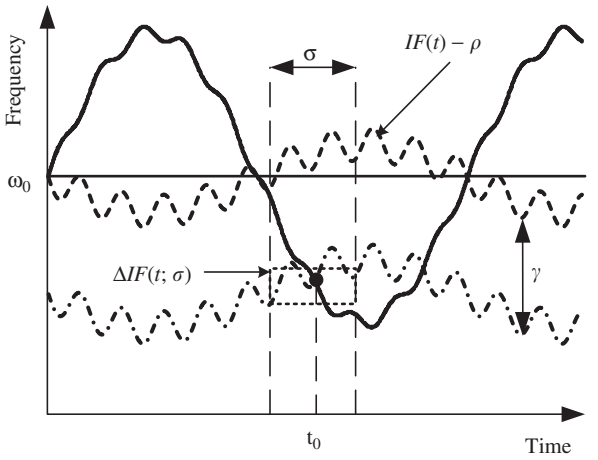

Fig. 5. The illustration of WBT (solid line: the IF law of the object chirp signal; dash line: after frequency rotation; dash dot line: after frequency shift).

IF can be approximated by the Fourier series. Since the prior knowledge about the signal is usually unknown in real applications, it is desired to determine the coefficients of the Fourier series kernel effectively and adaptively based on the objective signal. Fourier transform is a generalization of the complex Fourier series and the Fourier spectrum of a function is related to its Fourier coefficients. Therefore, a coefficients estimation method for the GWT is proposed using the Fourier spectrum of the objective IF. The relationship between the Fourier coefficients and the Fourier transform of the IF is given as follows:

$$F(n\omega_0)=\sum_{t=0}^{\infty}\mathrm{IF}(t)\exp(-jn\omega_0 t) \tag{12}$$

$$F(n\omega_0)=\begin{cases}\frac{1}{2}(a_n+j\beta_n) & \text{for} \quad \mathrm{n}<0\\ \frac{1}{2}a_0 & \text{for} \quad \mathrm{n}=0\\ \frac{1}{2}(a_n-j\beta_n) & \text{for} \quad \mathrm{n}>0\end{cases} \tag{13}$$

where ω_0 denotes fundamental frequency. n is an integer. $F(n\omega_0)$ denotes the Fourier transform of $IF(t)$; a_n and β_n are the Fourier coefficients.

The proposed coefficient estimation method aims to refine and estimate the coefficients of the Fourier series kernel of the GWT based on the signal under consideration. First, with the Fourier series kernel characteristic coefficients of $\{a_1,a_2,\ldots,a_m\}=\{0,0,\ldots,0\}_{1\times m}$ and $\{\beta_1,\beta_2,\ldots,\beta_m\}=\{0,0,\ldots,0\}_{1\times m}$, the GWT generates an TFR for the signal. Then, the position of the locally maximum energy in the TFR is extracted as estimated IF, i.e.,

$$\widetilde{IF}(t)=\underset{\omega}{\mathrm{argmax}}[|GWT(t_0,a,\beta,f,\omega;\sigma)|] \tag{14}$$

Third, the Fourier spectrum is obtained through the Fourier transform of the estimated IF, $\widetilde{IF}(t)$, and the Fourier coefficients can be calculated based on the spectrum according to Eqs. (12) and (13). With the obtained coefficients, the Fourier series kernel of the GWT is a better approximation of the objective IF so that the GWT can generate an improved TFR with better energy concentration. This procedure is iterated to refine the coefficients until no more evident change between two successive estimated IFs. The termination condition is expressed as follows:

$$\zeta=\quad \mathrm{mean}\quad\left[\int\frac{|\widetilde{\mathrm{IF}}_{\mathrm{i}+1}(\mathrm{t})-\widetilde{\mathrm{IF}}_{\mathrm{i}}(\mathrm{t})|}{|\widetilde{\mathrm{IF}}_{\mathrm{i}}(\mathrm{t})|}\mathrm{dt}\right]<\delta \tag{15}$$

where $\widetilde{IF}_i(t)$ denotes the estimated IF in the ith iteration and δ is a pre-defined threshold. The details of the coefficient estimation method for the GWT is given as follows.

3.1. The coefficient estimation method for the GWT

Initialization step:

Let $\{a_1a_2\ldots a_m\}=\{00\ldots0\}_{1\times m}$ and $\{\beta_1\beta_2\ldots\beta_m\}=\{00\ldots0\}_{1\times m}$, set δ, the window size, non-zero $\{f_1f_2\ldots f_m\}$, and the maximum iteration$k_{\max}$

While $k<k_{\max}$and $\zeta<\delta$

1. Generating the TFR for the analytical signal $z(t)$ by the GWT with $\{a_1 a_2 \ldots a_m\}$, $\{\beta_1 \beta_2 \ldots \beta_m\}$, and $\{f_1 f_2 \ldots f_m\}$.
2. Estimating $\widetilde{IF}_k(t)$ from the TFR generated in Step 1 according to Eq. (14).
3. Applying fast Fourier transform to $\widetilde{IF}_k(t)$ and estimating $\{a_1 a_2 \ldots a_m\}$, $\{\beta_1 \beta_2 \ldots \beta_m\}$, and $\{f_1 f_2 \ldots f_m\}$ according to Eqs. (12) and (13).
4. Updating $\{a_1 a_2 \ldots a_m\}$, $\{\beta_1 \beta_2 \ldots \beta_m\}$, and $\{f_1 f_2 \ldots f_m\}$.
5. Calculating the terminal condition ζ according to Eq. (15) and $k \leftarrow k+1$

End

In order to demonstrate the proposed coefficient estimation method for the GWT, a NLFM signal is considered as an example

$$s(t) = \sin\left(40\pi t - 200\pi \cos\frac{t}{10} - 6\pi \cos t\right) (0 < t < 60s) \tag{16}$$

whose IF law is

$$\omega(t) = 20 + 10\sin\frac{t}{10} + 3\sin t \ (\mathrm{Hz}) \tag{17}$$

A Gaussian noise is artificially added to the signal. The window size is set to be 512 and the threshold δ is 0.1%. Before reaching the termination condition, 4 iterations have been run. The obtained TFR as well as the estimated IF in each iteration are shown in Figs. 6–9. In the TFR illustrated in Fig. 6(a), it can be seen that only high energies are distributed at local extreme of the IF trajectory. In Fig. 6(b), a Fourier series is used to approximate the estimated IF and the coefficients of the Fourier series are estimated based on the spectrum of the estimated IF. Then, in the TFR generated by the GWT with the updated coefficients shown in Fig. 7(a), the energy is much more concentrated in the vicinity of the IF

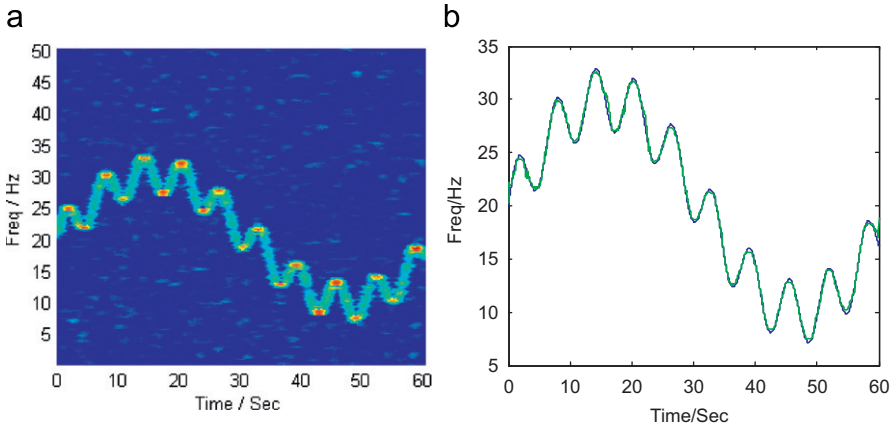

Fig. 6. (a) The TFR and (b) the estimated IF in the 1st iteration (blue line: the estimated IF; green line: the approximation of IF). (For interpretation of the references to color in this figure legend, the reader is referred to the web version of this article.)

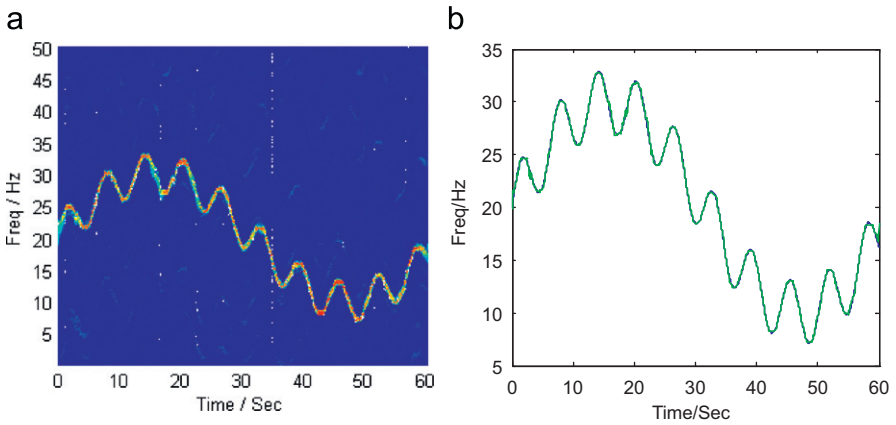

Fig. 7. (a) The TFR and (b) the estimated IF in the 2nd iteration (blue line: the estimated IF; green line: the approximation of IF). (For interpretation of the references to color in this figure legend, the reader is referred to the web version of this article.)

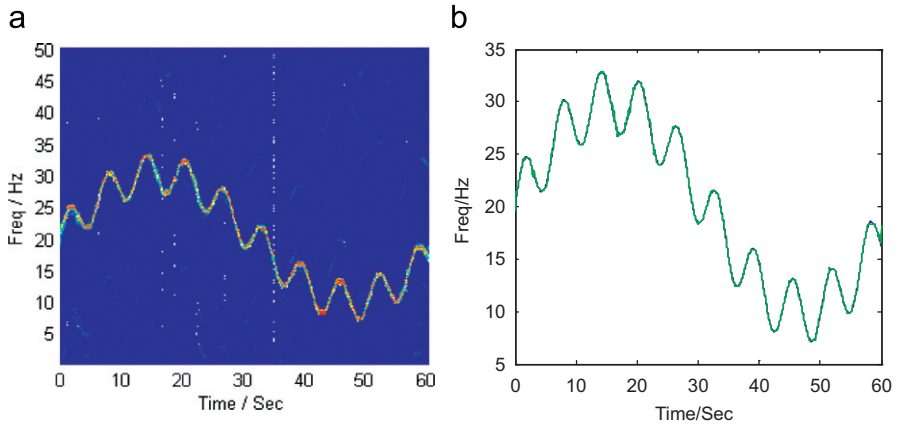

Fig. 8. (a) The TFR and (b) the estimated IF in the 3rd iteration (blue line: the estimated IF; green line: the approximation of IF). (For interpretation of the references to color in this figure legend, the reader is referred to the web version of this article.)

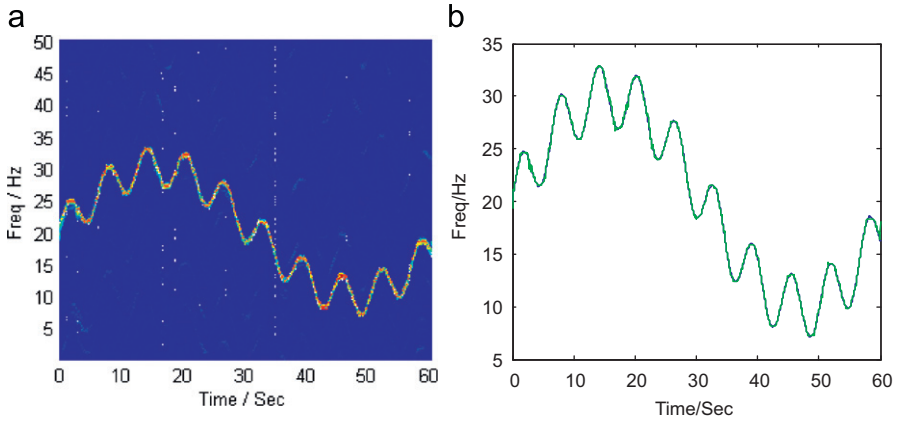

Fig. 9. (a) The TFR and (b) the estimated IF in the 4th iteration (blue line: the estimated IF; green line: the approximation of IF). (For interpretation of the references to color in this figure legend, the reader is referred to the web version of this article.)

Table 1
The value of termination condition.

Iteration number	2	3	4
ζ (%)	0.8686	0.1557	0.006

Table 2
Errors of the estimated IF comparing to true IF.

Iteration number	1	2	3	4
Error (%)	8.5839	3.1176	2.4940	2.2850

trajectory. In Figs. 8 and 9, it is expected that the TFR generated in the 3th and 4th iterations are improved in terms of energy concentration and more accurate IF estimations are obtained. In order to quantify the accuracy of the estimated IF, an error measurement between the estimated IF trajectory and the true IF trajectory is defined as follows:

$$\text{error} = \text{mean} \int [\widetilde{IF}_i(t) - IF(t)]^2 dt \tag{18}$$

The termination conditions and the errors are listed in Tables 1 and 2, respectively. It can be seen that the estimated IF becomes closer to the true IF of the signal, which testifies that the proposed coefficient estimation method is able to refine the coefficients of the Fourier series kernel to match the objective IF adaptively. It is worth noting that the number of

the sine and cosine functions of the Fourier series, m, can be adjusted to reach different approximation accuracy, i.e., fewer sine and cosine functions of the Fourier series results in smoother but less accurate approximation of the IF.

4. Validation

4.1. Numerical examples

In order to validate the performance of the proposed method, STFT, WT and WVD are considered for comparison purpose. In the tests on two numerical signals, the sampling frequency is set to be 100 Hz and window length is 1024.

The first signal is considered as

$$s(t)=\sin\left(20\pi t+2.5\pi t^2+\frac{2}{9}\pi t^3-\frac{1}{80}\pi t^4\right)(0<t<18s) \tag{19}$$

whose IF law is

$$f_{im}(t)=10+2.5t+(t^2/3)-(t^3/40)\ (\mathrm{Hz}) \tag{20}$$

The results are shown in Fig. 10. The coefficients of the Fourier series kernel of the GWT are obtained by the proposed coefficient estimation method. Only few coefficients are listed as follows due to the limit of space,

$$\begin{cases} \{a_1,a_2,a_3,a_4,a_5\}=[9.33,\ 2.01,\ 1.02,\ 0.68,\ 0.51] \\ \{\beta_1,\beta_2,\beta_3,\beta_4,\beta_5\}=[11.21,\ 2.78,\ 1.21,\ 0.67,\ 0.41] \\ \{f_1,f_2,f_3,f_4,f_5\}=[0.0555,0.1110,0.1666,0.2221,0.2776] \end{cases} \tag{21}$$

The TFR generated by the STFT illustrated in Fig. 10(a) shows poor energy concentration in the time-varying proportion of the IF due to the constant time-frequency resolution. In the TFR generated by the WT illustrated in Fig. 10(b), the energy spreads over the high frequency range, i.e., around 45 Hz, for the coarser frequency resolution provided by the WT. The WVD can generate a TFR with the best energy concentration for the LFM signal. However, in the TFR generated by the

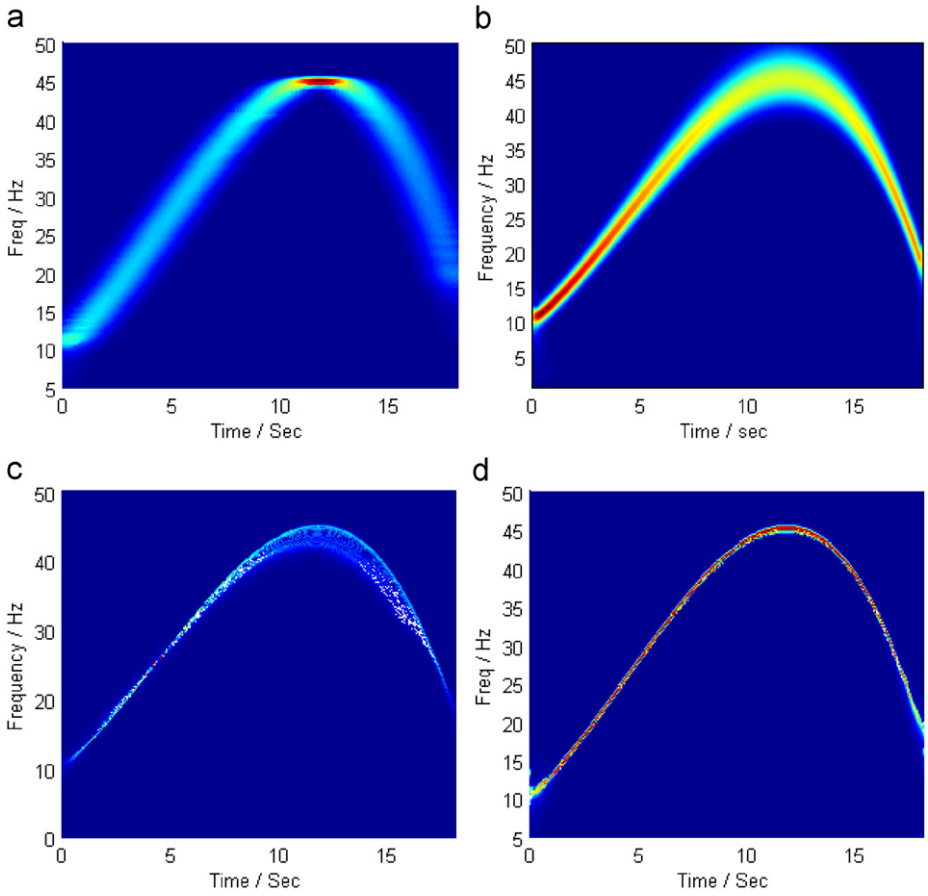

Fig. 10. The TFR of the 1st numerical example generated by (a) the STFT, (b) the WT, (c) the WVD and (d) the GWT.

WVD shown in Fig. 10(c), the bilinear structure of the WVD introduces the cross-terms at the high frequency range. On the other hand, it can be seen that the TFR generated by the GWT has the energy extremely concentrated along the IF trajectory and outperforms the other three methods in characterizing the true time-frequency pattern of the objective signal.

The second example considers a signal, whose IF law is given by

$$\omega(t) = 10 + \frac{24}{\pi}\left[\sin(t) + \frac{1}{3}\sin(3t) + \frac{1}{5}\sin(5t) + \frac{1}{7}\sin(7t)\right] \text{ (Hz)} \tag{22}$$

i.e.,

$$s(t) = \sin\left\{20\pi t - 2\pi \times \frac{24}{\pi}\left[\cos(t) + \frac{1}{9}\cos(3t) + \frac{1}{25}\cos(5t) + \frac{1}{49}\cos(7t)\right]\right\} (0 \le t \le 15s) \tag{23}$$

The TFRs generated by the STFT, WT, WVD and the GWT are shown in Fig. 11. It can be seen in Fig. 11(a) that the IF trajectory characterized by the STFT loses the details at flat areas of 4 and 16 Hz. Meanwhile, the TFR generated by the STFT shows extraordinary energy leakage when the IF changes rapidly with time, i.e., rigid zone between 4 and 16 Hz. Thus, the STFT with the fixed time-frequency resolution is not adequate to analyze non-stationary signals. In the TFR obtained by the WT shown in Fig. 11(b), the energies are scattered at higher frequency due to the coarser frequency resolution, and the IF trajectory is blurred at lower frequency for the coarser time resolution. In the TFR generated by the WVD shown in Fig. 11(c), the superior frequency components of the cross-terms make the accurate identification of the objective IF impossible. On the contrary, the promising result obtained by the GWT is shown in Fig. 11(d). It can be seen that the TFR has excellent energy concentration along the IF trajectory and characterizes the true time-frequency pattern of the signal.

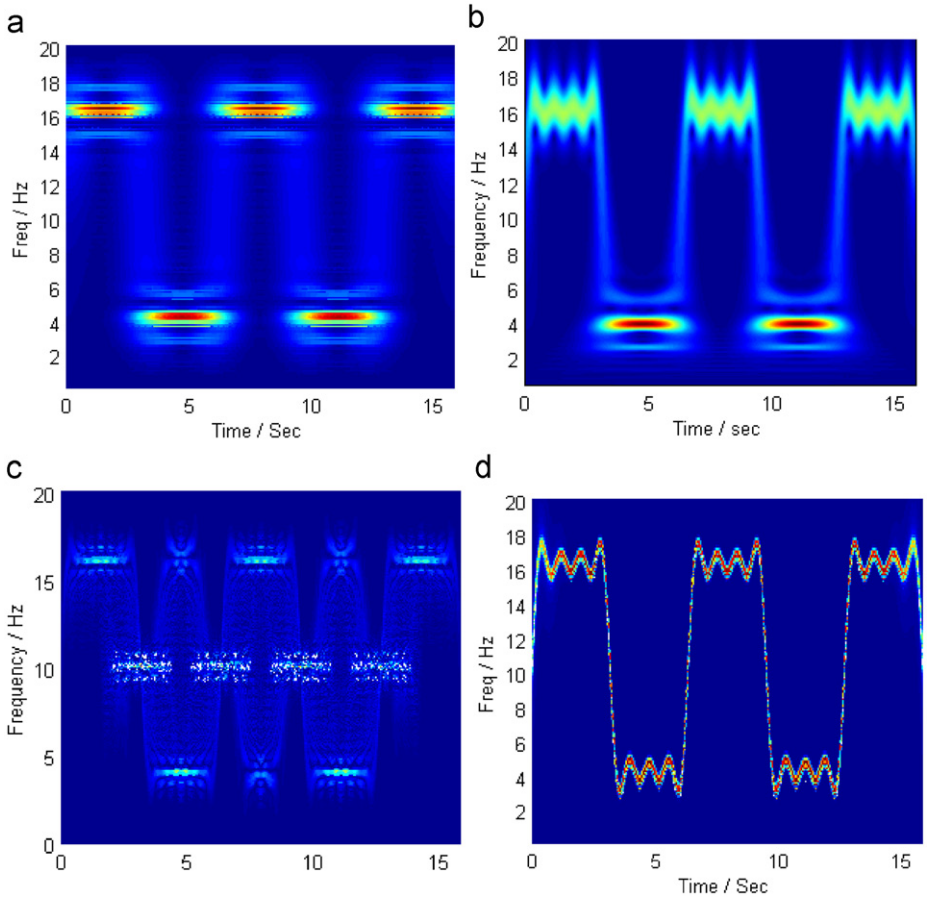

Fig. 11. The TFR of the 2nd numerical example generated by (a) the STFT, (b) the WT, (c) the WVD and (d) the GWT.

The coefficients of the Fourier series kernel of the GWT for the signal are listed as follows:

$$\begin{cases} \{a_1, a_2, a_3, a_4\} = -\frac{24}{\pi}\left[1, \frac{1}{3}, \frac{1}{5}, \frac{1}{7}\right] \\ \{\beta_1, \beta_2, \beta_3, \beta_4\} = [0, 0, 0, 0] \\ \{f_1, f_2, f_3, f_4\} = \left[\frac{1}{2\pi}, \frac{3}{2\pi}, \frac{5}{2\pi}, \frac{7}{2\pi}\right] \end{cases} \tag{24}$$

4.2. Transient vibration signal undergoing speed-up and slow-down stages

As rotating machine is increasingly employed in complex continuous operation, condition monitoring is an effective way to increase the productivity and reliability, as well as facilitate the prognostics and maintenance for the rotating machine in manufacturing process. Speed-up and slow-down processing is often related to the change of the machine speeds and loads, which contains valuable information of the machine health. Thus, it is desirable to monitor the vibration behavior of the rotating machine during the transient processes. The vibration signal of the machine during these processes is typically transient along with frequency modulation. The time-frequency analysis of such vibration signals has received broad attentions [15,33,34].

To validate the proposed method, a set of the vibration signal collected from a rotor test rig undergoing speed-up and slow-down stages is used. The test rig is shown in Fig. 12. A set of the collected vibration signal is shown in Fig. 13. The sampling frequency is set to be 100 Hz and the window size is 512. The termination condition in Eq. (15) is applied and the threshold is $\delta = 0.1\%$. Three iterations have been run before reaching the termination condition. The TFRs and the estimated instantaneous speed obtained by the STFT and the SCT are shown in Figs. 14 and 15, respectively. Comparing to the STFT,

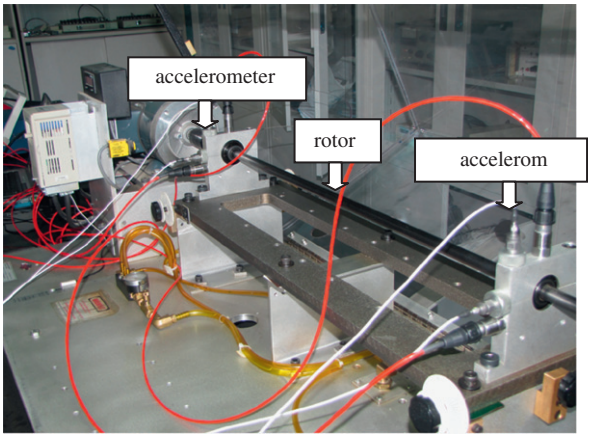

Fig. 12. The rotor test rig.

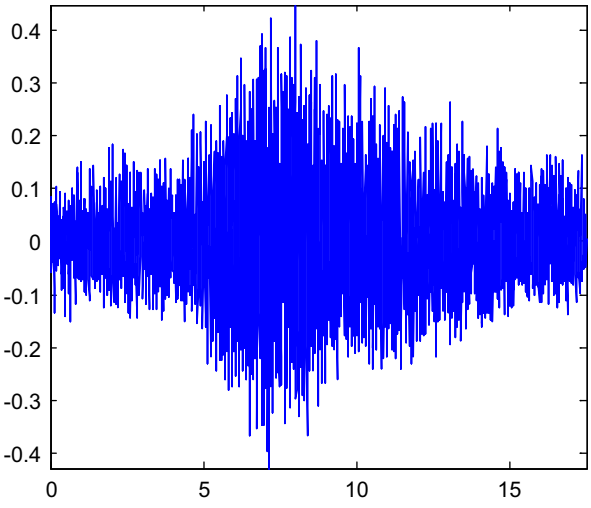

Fig. 13. A set of vibration signal.

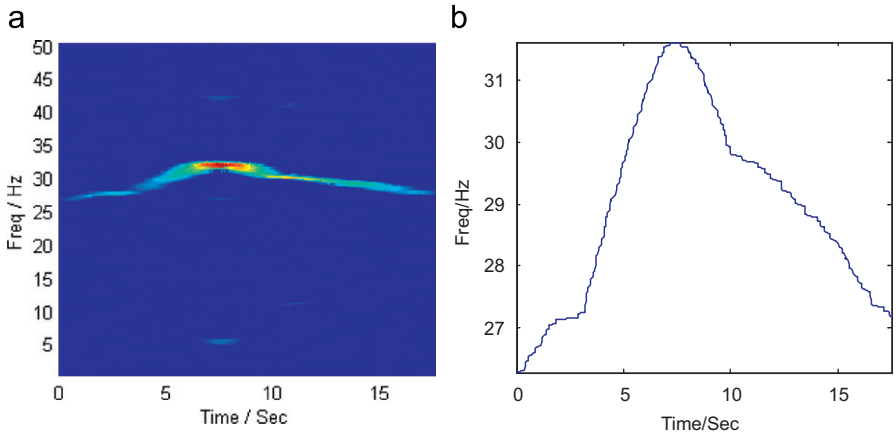

Fig. 14. (a) The TFR and (b) instantaneous speed estimation obtained by STFT.

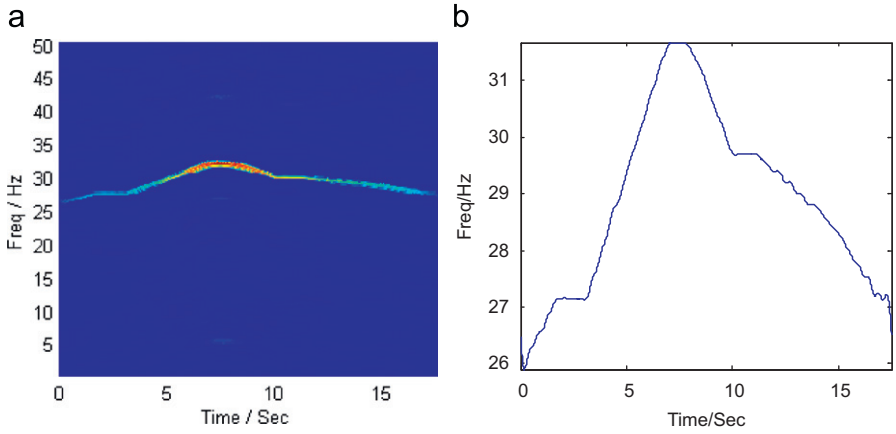

Fig. 15. (a) The TFR and (b) instantaneous speed estimation obtained by GWT.

the TFR generated by the GWT has much better energy concentration along the fundamental frequency component of the rotor system, which is nonlinearly varying with time. Therefore, the GWT can guarantee accurate estimation of the instantaneous frequency for the rotor system.

It should be noticed that the proposed GWT focuses on mono-component signals, in another words, the GWT is currently not suitable to analyze the multi-component signal with multiple frequency components that need to be approximated with different Fourier series. This is a common problem for the parameterized time-frequency transforms. The authors are now working on extending the GWT to analyze the multi-component signal from a post-processing point of view, which will be presented in the future.

5. Conclusion

In this paper, a generalized Warblet transform (GWT) is proposed to characterize the time-frequency pattern of the signal with arbitrary highly oscillating IF that can be approximated by Fourier series. Unlike the conventional time-frequency transforms, the GWT is able to provide fine frequency resolution and avoid interference of cross-terms for non-stationary signals whose IF can be periodic or non-periodic. Moreover, the developed signal-dependent coefficient estimation method practically facilitates the GWT to obtain a TFR with excellent energy concentration and achieve an accurate IF estimation. The effectiveness of the proposed method is verified by the analysis of both artificial examples and experimental signal. The results show that the GWT outperforms STFT, WT and WVD in providing the TFR with excellent energy concentration and the accurate IF estimation for the signal with arbitrary highly oscillating IF, which can be periodic or non-periodic. The future work directs to enable the proposed method to analyze multi-component signals in real applications.

Acknowledgments

The authors gratefully acknowledge that the work was supported by the Natural Science Foundation of China (Nos. 10902068 and 10732060), Shanghai Pujiang Program (10PJ1406000), the Research Fund of State Key Lab of MSV, China (Grant no. MSV-ZD-2010-01) and the Program for NCET in universities of China (No. NCET-10-0548) for this work.

References

[1] J. Carson, T. Fry, Variable frequency electric circuit theory with application to the theory of frequency modulation, Bell System Technical Journal 16 (1937) 513–540.
[2] D. Gabor, Theory of communication. Part 1: The analysis of information, electrical engineers—part III: radio and communication engineering, Journal of the Institution 93 (1946) 429–441.
[3] J. Ville, Theory and applications of the notion of complex signal, RAND Corporation, 1958.
[4] C. Ioana, A. Jarrot, C. Gervaise, et al., Localization in underwater dispersive channels using the time-frequency-phase continuity of signals, IEEE Transactions on Signal Processing 58 (2010) 4093–4107.
[5] N. stlund, Y. Jun, J. Karlsson, Improved maximum frequency estimation with application to instantaneous mean frequency estimation of surface electromyography, IEEE Transactions on Biomedical Engineering 51 (2004) 1541–1546.
[6] R. Zivanovic, An adaptive differentiation filter for tracking instantaneous frequency in power systems, IEEE Transactions on Power Delivery 22 (2007) 765–771.
[7] J. Astola, K. Egiazarian, G. Khlopov, et al., Application of bispectrum estimation for time-frequency analysis of ground surveillance Doppler radar echo signals, IEEE Transactions on Instrumentation and Measurement 57 (2008) 1949–1957.
[8] S. Anderson, K. Sabra, M. Zakharia, et al., Timefrequency variations of the bistatic scattering response of proud and buried elastic shells in shallow water: implication for mine counter-measure sonar systems, The Journal of the Acoustical Society of America 124 (2008) 2520-2520.
[9] C. Ibars, Y. Bar-Ness, Analysis of time–frequency duality of MC and DS CDMA for multiantenna systems on highly time-varying and wide-band channels, IEEE Transactions on Wireless Communications 4 (2005) 2661–2667.
[10] M. An, A. Brodzik, R. Tolimieri, Ideal Sequence Design in Time-Frequency Space: Applications to Radar, Sonar, and Communication Systems, Birkhauser, 2008.
[11] F. Nathanson, J. Reilly, M. Cohen, Radar Design Principles: Signal Processing and the Environment, SciTech Publishing, 1999.
[12] Z. Ge, P. Huang, W. Lu, Matched NLFM Pulse Compression Method with Ultra-low Sidelobes, EuRAD 2008. European, 2008, 92–95.
[13] T. Collins, P. Atkins, Nonlinear frequency modulation chirps for active sonar, IEE Proceedings-Radar, Sonar and Navigation 146 (1999) 312–316.
[14] W. Shuozhong, M.L. Grabb, T.G. Birdsall, Design of periodic signals using FM sweeps and amplitude modulation for ocean acoustic travel-time measurements, Oceanic Engineering, IEEE Journal of oceanic engineering 19 (1994) 611–618.
[15] S. Rajagopalan, J.M. Aller, J.A. Restrepo, et al., Detection of rotor faults in brushless DC motors operating under nonstationary conditions, IEEE Transactions on Industry Applications 42 (2006) 1464–1477.
[16] S. Qian, D. Chen, Joint time-frequency analysis, IEEE Signal Processing Magazine 16 (1999) 52–67.
[17] B. Boashash, Time Frequency Signal Analysis and Processing: a Comprehensive Reference, Elsevier Science Ltd., 2003.
[18] H. Kwok, D. Jones, Improved instantaneous frequency estimation using an adaptive short-time Fourier transform, IEEE Transactions on Signal Processing 48 (2000) 2967–2972.
[19] P. Boggiatto, G. Donno, A. Oliaro, A class of quadratic time-frequency representations based on the short-time Fourier transform, Modern Trends in Pseudo-Differential Operators 172 (2007) 235–249.
[20] R. Scheper, A. Teolis, Cramer–Rao bounds for wavelet transform-based instantaneous frequency estimates, IEEE Transactions on Signal Processing 51 (2003) 1593–1603.
[21] J. Beltrán, J. Ponce de León, Estimation of the instantaneous amplitude and the instantaneous frequency of audio signals using complex wavelets, Signal Processing 90 (2010) 3093–3109.
[22] H. Hong, M. Liang, Separation of fault features from a single-channel mechanical signal mixture using wavelet decomposition, Mechanical Systems and Signal Processing 21 (2007) 2025–2040.
[23] P. Shui, H. Shang, Y. Zhao, Instantaneous frequency estimation based on directionally smoothed pseudo-Wigner–Ville distribution bank, Radar, Sonar & Navigation, IET 1 (2007) 317–325.
[24] B. Barkat, B. Boashash, Instantaneous frequency estimation of polynomial FM signals using the peak of the PWVD: statistical performance in the presence of additive Gaussian noise, IEEE Transactions on Signal Processing 47 (1999) 2480–2490.
[25] L. Gelman, J.D. Gould, Time-frequency chirp-Wigner transform for signals with any nonlinear polynomial time varying instantaneous frequency, Mechanical Systems and Signal Processing 21 (2007) 2980–3002.
[26] S. Mann, S. Haykin, C. MIT, The chirplet transform: physical considerations, IEEE Transactions on Signal Processing 43 (1995) 2745–2761.
[27] L. Gelman, M. Ottley, New processing techniques for transient signals with non-linear variation of the instantaneous frequency in time, Mechanical Systems and Signal Processing 20 (2006) 1254–1262.
[28] F. Peng, D. Yu, J. Luo, Sparse signal decomposition method based on multi-scale chirplet and its application to the fault diagnosis of gearboxes, Mechanical Systems and Signal Processing 25 (2011) 549–557.
[29] L. Angrisani, M. D'Arco, R. Moriello, et al., On the use of the warblet transform for instantaneous frequency estimation, IEEE Transactions on Instrumentation and Measurement 54 (2005) 1374–1380.
[30] L. Angrisani, M. D'Arco, A measurement method based on a modified version of the chirplet transform for instantaneous frequency estimation, IEEE Transactions on Instrumentation and Measurement 51 (2002) 704–711.
[31] L. Angrisani, M. D'Arco, R. Moriello, et al., Warblet transform-based method for instantaneous frequency measurement on multicomponent signals, International Journal of Information Systems and Telecommunication Engineering 1 (2010) 50–59.
[32] W. Yang, Interpretation of mechanical signals using an improved Hilbert–Huang transform, Mechanical Systems and Signal Processing 22 (2008) 1061–1071.
[33] D. Shi, F. Tsung, P. Unsworth, Adaptive time-frequency decomposition for transient vibration monitoring of rotating machinery, Mechanical Systems and Signal Processing 18 (2004) 127–141.
[34] S. Rajagopalan, J. Restrepo, J. Aller, et al., Nonstationary motor fault detection using recent quadratic time–frequency representations, IEEE Transactions on Industry Applications 44 (2008) 735–744.